NHTSA OBLIQUE CRASH TEST RESULTS: VEHICLE PERFORMANCE AND OCCUPANT INJURY RISK ASSESSMENT IN VEHICLES WITH SMALL OVERLAP COUNTERMEASURES

James Saunders
Dan Parent
Eva Ames
National Highway Traffic Safety Administration (NHTSA)
USA
Paper Number: 15-0108

ABSTRACT

Objective: The National Highway Traffic Safety Administration (NHTSA) has been developing a research test protocol representative of real-world injury potential in frontal offset oblique impacts. This paper will address the vehicle and occupant responses from the latest research test series.
Methods: In this series, the Oblique Moving Deformable Barrier (OMDB) impacted stationery vehicles in both left and right side impacts. Vehicles were selected only if their performance in the Insurance Institute for Highway Safety (IIHS) Small Overlap (SOI) test condition earned a "Good" or "Acceptable" rating and had side curtain air bags meeting the requirements of Federal Motor Vehicle Safety Standard (FMVSS) No. 226, Ejection Mitigation. The vehicle responses studied included total velocity change (delta-V, DV), interior intrusion and steering wheel displacement, and the occupant responses studied included Brain Injury Criterion (BrIC), Multipoint Thoracic Injury Criterion, and Ankle Moment.
Results: Generally, delta-V (DV) in the X-direction decreased as the weight of the vehicle increased in both left and right side impacts, and the interior intrusion increased toward the center of the vehicle for both impact directions as well. A significant correlation between lap belt loads and vehicle mass was not found, but there was a general decreasing trend of peak lap belt loads with increase in vehicle mass. Occupant kinematics were generally mirror images for left and right side impacts, with the occupant's head moving forward and toward the direction of impact. The near-side occupants' heads moved toward the gap between the frontal and side curtain air bags, while the far-side occupants' heads rotated off of the frontal air bag and impacted the center instrument panel.
Discussion: The Honda Accord showed the greatest difference between left and right side impact vehicle response. The highest probability of injury for both near- and far-side occupants was predicted to occur in the head, chest, and ankle, agreeing with the findings from previous real-world oblique crash injury analysis. The test mode predicted a high risk of ankle injury, primarily due to ankle inversion and/or eversion. Left and right side impacts resulted in similar magnitudes of vehicle response, but occupant responses differed enough that it may be important to consider both left and right side oblique impacts in restraint system design.
Conclusions: The interior intrusions on the toe pan increased towards vehicle center, and toe pan point TP3 consistently showed the highest intrusion measurement. Vehicle deformation from left and right side impacts can differ due to the stack up of non-symmetrical vehicle component layouts. The latest NHTSA Oblique test series involving vehicles with a "Good" or "Acceptable" rating in the IIHS SOI test condition and with side curtain air bags meeting the requirements of FMVSS No. 226 suggest that additional countermeasures may reduce injury risk in this test mode.

INTRODUCTION

A September 2009 report from the National Highway Traffic Safety Administration (NHTSA) investigated why occupant fatalities still occur in frontal crashes despite the presence of air bags and seat belts and the crashworthy structures of late-model vehicles [1]. It concluded that, aside from exceedingly severe crashes, the main cause of these deaths was poor structural engagement between the vehicle and its collision partner: corner impacts, oblique crashes, impacts with narrow objects, and heavy vehicle underrides. In response, the agency initiated a research program to develop a crash test procedure capable of replicating the injury potentials from real-world frontal offset oblique crashes.

The NHTSA Research Oblique Crash Test Protocol, illustrated below in Figure 1, involves a moving deformable barrier (MDB) weighing 2,486 kg (5,480 lb) which impacts a stationary vehicle at a speed of 90 km/h (56 mph), a 15 degree angle, and a 35 percent overlap. For an average mass 1,497 kg (3,300 lb) target vehicle, this barrier-to-vehicle crash has a delta-V of 56 km/h (35 mph), which is equivalent to a crash between two average mass vehicles with the bullet vehicle striking the target vehicle at a speed of 113 km/h (70 mph), a 15 degree angle, and a 50 percent overlap. For this test, a THOR 50th percentile male anthropomorphic test device (ATD) is seated in both the driver's and front passenger's positions.

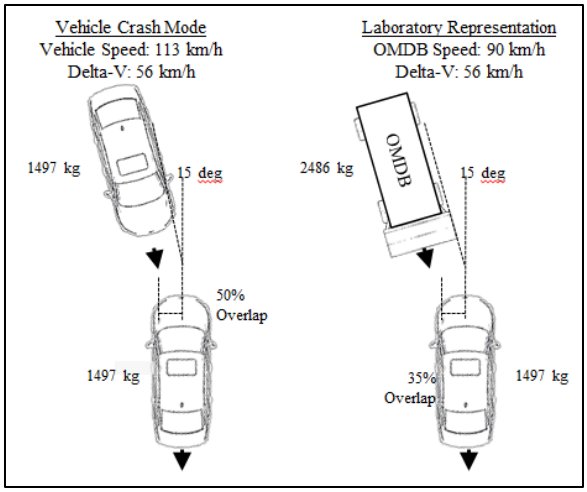

Figure 1. Test Setup

This test method is different from the existing New Car Assessment Program (NCAP) frontal tests in which the amount of test energy depends upon the mass of the vehicle. Because of the MDB impacting a stationary vehicle at the same speed regardless of the target vehicle's mass, the NHTSA Research Oblique Test Protocol is a constant-energy test, which encourages comparison of vehicle safety results between vehicle classes. As explained in Saunders 2012, the test speed was selected for consistency with the test severity of the NCAP frontal crash [2]. Saunders 2012 mistakenly noted that the NCAP test speed was 90 km/h (56 mph), but the proper speed, 56 km/h (35 mph), was actually used for the derivation of the speed for the NHTSA Oblique Test Protocol.

The research program started with a series of full-scale vehicle-to-vehicle crash tests to establish a baseline understanding of vehicle interaction and occupant kinematics. These full-scale vehicle-to-vehicle tests were then compared to results obtained in crash tests using an MDB, where it was determined that the MDB already in use in Federal Motor Vehicle Safety Standard (FMVSS) No. 214 would require modifications to produce equivalent test results. The face plate was enlarged to a width greater than the outer barrier track width to prevent wheel damage, a suspension was added to prevent the assembly from bouncing at high speeds, and the barrier honeycomb stiffness and thickness were optimized to prevent the barrier face from bottoming out too soon [3]. This modified version of the FMVSS No. 214 MDB is called the Oblique Moving Deformable Barrier (OMDB).

Previously, test procedure repeatability was demonstrated [4] and vehicle crash tests of high sales volume vehicles were performed to expand the database of OMDB-to-vehicle crash tests with THOR 50th ATDs [5]. Testing of vehicles redesigned or introduced in 2010 and 2011 with the highest ratings in US consumer rating programs has shown that there is potential for additional vehicle design improvements to mitigate real-world injuries and fatalities in frontal oblique crashes [5]. When comparing the average injury assessment values (IAVs) for each body region, trends appeared which mirrored the real-world data, including the risk of knee-thigh-hip, lower extremity, head, and chest injuries. Rudd, et al. 2011 also found similar injury incidence when they reviewed oblique crashes included in the Crash Injury Research and Engineering Network (CIREN) and National Automotive Sampling System Crashworthiness Data System (NASS-CDS) databases [6].

The current study presents both vehicle and occupant results from the latest series of OMDB-to-vehicle crash tests, in which vehicle selection was limited to those which received a "Good" or "Acceptable" rating in the Insurance Institute for Highway Safety (IIHS) Small Overlap Impact (SOI) crash test and also had side curtain air bags meeting the requirements of Federal Motor Vehicle Safety Standard (FMVSS) No. 226, "Ejection mitigation." These NHTSA Oblique tests were performed in both the left side impact (LSI) and right side impact (RSI) conditions, and kinematics for the occupants on both the struck and non-struck sides were evaluated.

METHODOLOGY

Oblique Crash Testing

Figure 21, in APPENDIX A, shows the left side impact (LSI) Oblique test procedure setup. In this setup, the OMDB impacts the target vehicle at 90 km/h (56 mph) and the stationary vehicle is positioned such that the angle between the OMDB and the vehicle is 15 degrees clockwise and the overlap is 35 percent on the driver side of the vehicle. For right side impacts (RSI) the OMDB impacts the target vehicle at 90 km/h (56 mph) and the stationary vehicle is positioned such that the angle between the OMDB and the stationary vehicle is 15 degrees counterclockwise and the overlap is 35 percent on the passenger side of the vehicle.

The vehicles were instrumented with a rear accelerometer on the left and right door sill to record the X and Y accelerations of the vehicle. APPENDIX B describes the intrusion points taken during the test. These points where placed according to IIHS "Moderate Overlap Frontal Crashworthiness Evaluation Crash Test Protocol (Version XV) dated May 2014. These points are listed in Table 3 and illustrated in Figure 23 and Figure 24, in APPENDIX B.

Table 1 shows the list of vehicles tested in the LSI condition, along with the naming convention for each vehicle, and Table 2 shows the list of vehicles tested in the RSI condition.

Table 1: LSI matrix and vehicle naming convention

NHTSA TEST NUMBER	MAKE	MODEL	YEAR	TEST WEIGHT (KG)
9043	Honda	Fit	2015	1426
8787	Mazda	3	2014	1588
8789	Honda	Accord	2014	1744
8788	Mazda	CX-5	2014	1769
8478	Subaru	Forester	2014	1803
8488	Volvo	S60	2012	1936

Table 2: RSI matrix and vehicle naming convention

NHTSA TEST NUMBER	MAKE	MODEL	YEAR	TEST WEIGHT (KG)
8999	Mazda	3	2014	1582
9042	Honda	Accord	2014	1749
8998	Mazda	CX-5	2014	1777

Occupant Response Assessment

Previous OMDB crash tests have included either a single THOR (Test Device for Human Occupant Restraint) anthropomorphic test device (ATD) seated in the driver (near-side) position, or THOR ATDs in both the driver and right front passenger positions. The tests presented in this paper (Table 1 and Table 2) included two THOR ATDs, one in the driver position and one in the right front passenger position. Both THOR ATDs met the specifications of the Mod Kit [7] with the addition of the SD-3 shoulder, a derivation of the Chalmers shoulder [8] which was further developed through the European Union's THORAX project [9]. For the LSI tests, the driver was on the near-side and the passenger on the far-side, while for the RSI tests, the passenger was on the near-side and the driver was on the far-side (further illustrated in Figure 22, APPENDIX A). In both the LSI and the RSI conditions, each ATD was positioned using the basic principles of the FMVSS No. 208 seating procedure, updated to account for the differences between THOR and Hybrid III.

Injury Criteria

Occupant injury risk was assessed by determining the probability of given severity of injury based on the Abbreviated Injury Scale (AIS) [10] [11]. For the head, neck, chest, abdomen, femur, and acetabulum, the probability of an AIS score of three or higher (AIS $\geq$ 3) was calculated. For the lower extremity, the probability of an AIS score of two or higher (AIS $\geq$ 2) was calculated. As such, this injury assessment was limited to injury criteria for which injury risk functions were available in the literature. Table 8, in APPENDIX G, summarizes the calculation of each injury criterion, including the predictor variable, any intermediate variables and constant definitions, and the associated injury risk functions. Compared to previous NHTSA publications of Oblique test results and analysis, there are three notable changes to calculation of injury risk.

BrIC. Previous analysis of brain injury risk in the Oblique test condition was calculated using the kinematic brain injury criterion (BRIC) injury assessment metric calculated using the method and critical values described in Saunders et al., 2012 [2]. Since that publication, an updated methodology for brain injury assessment was published

by Takhounts et al., 2013 [12]. The revised rotational brain injury criterion (BrIC) does not consider angular acceleration, but does consider each individual local axis of angular velocity. The critical values are directionally dependent but not dummy-specific, so the critical values applicable to THOR are the average critical angular velocities for the BrIC formulation based on maximum principle strain (MPS), as summarized in Table 8 (APPENDIX G).

Multipoint Thoracic Injury Criterion. A relationship between chest deformation and injury risk was determined through a series of matched-pair sled tests conducted at the University of Virginia [13]. Sled tests were conducted in twelve conditions using the THOR ATD with SD-3 shoulder, for which thoracic biofidelity has been demonstrated [14]. The matched set of post-mortem human surrogate (PMHS) tests included 38 observations on 34 PMHS (four PMHS were subjected to a low-speed, non-injurious loading condition before injurious testing). A relationship was developed between the thoracic deflections measured in the THOR ATD tests to the incidence of injury in the PMHS in the same condition. Thoracic deflection was quantified by calculating the maximum resultant deflection at any of the four measurement locations on the THOR rib cage. Incidence of injury was quantified as AIS $\geq$ 3 thoracic injury to the PMHS, which represents three or more fractured ribs based on the 2005 (update 2008) version of AIS. The paired PMHS and THOR tests, along with associated test number in the NHTSA Biomechanics Database where available and the peak resultant deflection measured by the THOR ATD in each condition, are included in Table 7 (APPENDIX F).

Ankle Moment. Kuppa et al., 2001 proposed injury risk curves for the human lower extremity [15] and described their application to the lower extremity hardware of the THOR ATD [16]. Injury risk function were presented for the prediction of tibia plateau fractures (proximal or upper tibia axial force), tibia/fibula shaft fractures (Revised Tibia Index), calcaneus, talus, ankle, and midfoot fractures (distal or lower tibia axial force), and malleolar fractures and ankle ligament injuries (ankle rotation angle or moment). Previous analyses of ankle injury in the Oblique test condition were discarded due to measured ankle rotation data that were inconsistent with visual ankle kinematics from review of high-speed video. Since malleolar and ankle ligament injuries account for 60 percent of the lower extremity injuries in air bag equipped vehicles in frontal crashes, ankle injury risk was revisited by calculating ankle dorsiflection moment and inversion/eversion moment as described by Kuppa et al., 2001 [16].

RESULTS

Vehicle Response

In general, the total velocity change (delta-V (DV)) in the X-direction decreased as the weight of the vehicle increased for both LSI and RSI (Figure 2). The DV in the X-direction for the vehicles impacted on the RSI was higher than the DV for LSI impacts, but the same trend held for weight.

Figure 3 and Figure 4 show the interior intrusion of the vehicles tested in both LSI and RSI. Generally, intrusion increased toward the center of the vehicle for both RSI and LSI. Also, for the toe pan, point TP3 always displayed the highest intrusion. There was no apparent trend for the Left IP, Right IP, bottom A-pillar, and rocker panel intrusions.

Figure 5 shows the residual displacement of the steering wheel in the X-Y plane of the vehicle. From this figure it can be seen that the steering wheel moves toward the driver's door, and the Forester had about 100 mm of displacement toward the door.

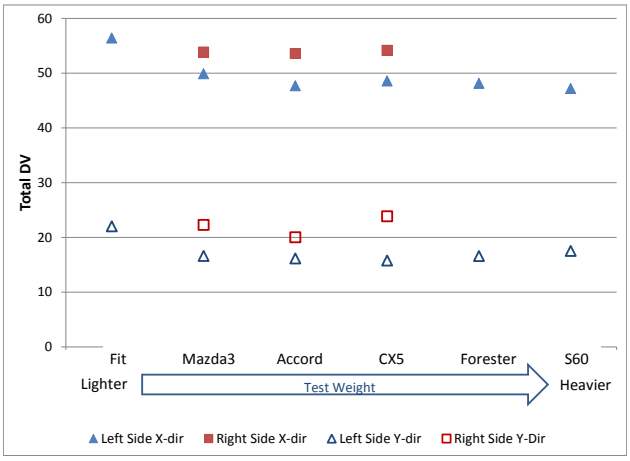

Figure 2. X DV

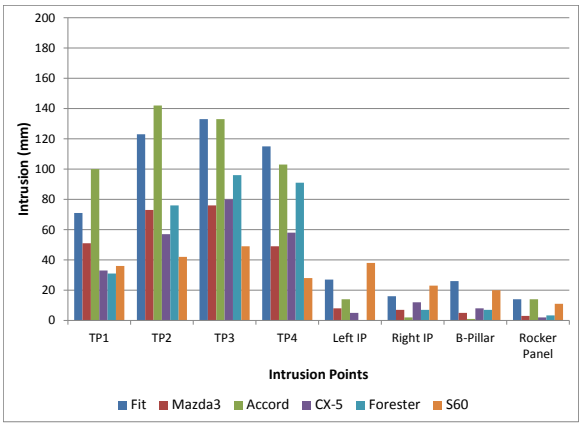

Figure 3 – Interior intrusions for LSI

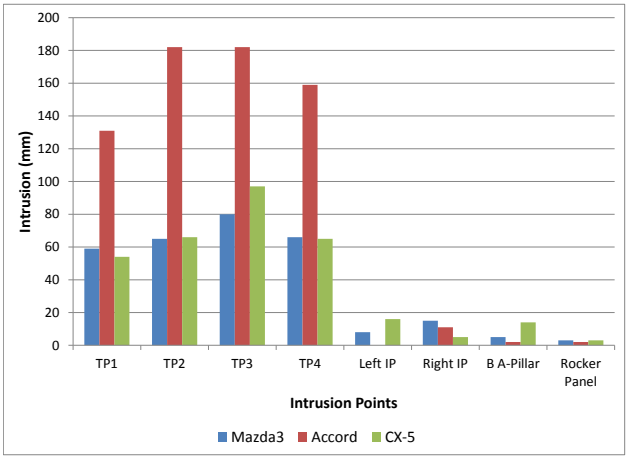

Figure 4 – Interior intrusions for RSI

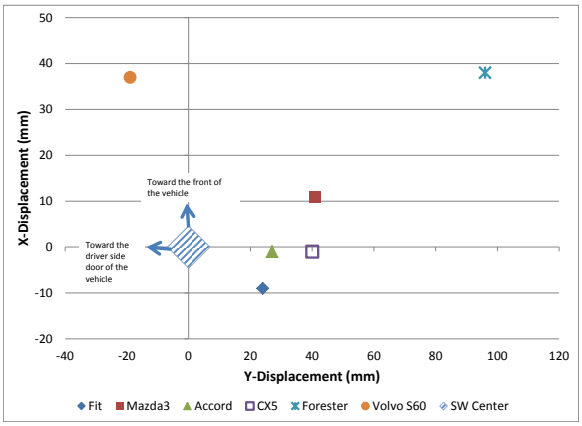

Figure 5 – Steering wheel motion in the X-Y plane

Occupant Response

Restraint Deployment. In all nine tests presented in this paper (Table 1 and Table 2), the vehicles deployed retractor pretensioners, frontal air bags, and side curtain air bags to the near-side occupants. The vehicles deployed retractor pretensioners and frontal air bags to the far-side occupants. Since the far-side occupants primarily translated and rotated in the inboard direction, the far-side curtain air bags were disabled to allow for high-speed video coverage.

Frontal air bag deployment time varied across vehicles, but deployed no later than 22 milliseconds after barrier contact with the bumper of the target vehicle. Safety belt pretensioners triggered at roughly the same time as frontal air bag deployment, and triggered at the same time for both the driver and right front passenger. The side curtain air bags generally deployed later than the frontal air bags, the outliers being the Forester (25ms) and the S60 (18ms) which fired at similar times to the frontal air bags. Restraint deployment times and head contact locations are summarized in Table 4 (APPENDIX C). Note that in some cases, contact was not evidenced by paint transfer since either the air bag itself or the hand shielded the contact between the head and door panel or instrument panel, but there was evidence of contact in the high-speed video and head acceleration time-histories.

In this set of vehicles, there was a general decreasing trend of peak lap belt loads with increase in vehicle mass (Figure 7), likely resulting from the decrease in delta-V with increasing mass (Figure 2). Overall there is not a significant correlation between lap belt loads and vehicle mass. If the near-side occupants are isolated, there is a statistically-significant relationship between peak lap belt force and vehicle mass ($p = 0.036$), but not for the far-side

occupants (p = 0.154). The far-side occupant saw a higher peak lap belt load than the near-side occupant in all but one vehicle, which had the highest shoulder belt load of the group (Forester, as seen in Figure 6). Despite the shoulder of the far-side occupant slipping out of the shoulder belt in every instance, far-side shoulder belt peak forces were higher than equivalent near-side shoulder belt forces, where the shoulder belt was retained throughout the event, in almost half of the observations. There was no apparent relationship between shoulder belt forces and any vehicle parameters, which is not surprising since shoulder belt forces are controlled by load limiters in all of the present vehicles with the exception of the Forester.

To examine whether the high shoulder belt load seen in the Forster was anomalous or the result of a malfunction, the shoulder belt loads from a frontal rigid barrier test of the 2014 Forester were reviewed (NHTSA vehicle database test number 8313) and found to be similarly high at 6,640 N. Thus, the Forester may have a higher load limit for the driver-side seating position than the other vehicles in this group. The second-highest shoulder belt force occurred in the Honda Fit far-side occupant location, but a similar 50th percentile male test is not available for comparison.

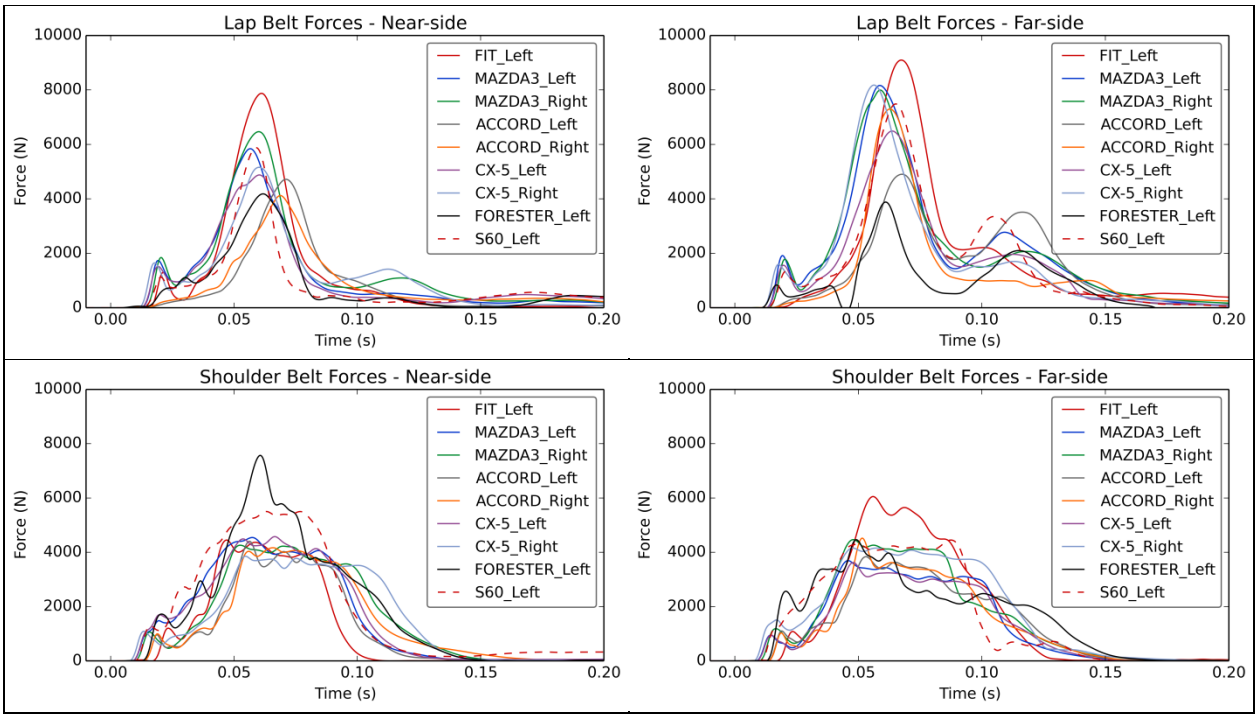

Figure 6. Lap and shoulder belt forces for the near- and far-side occupants.

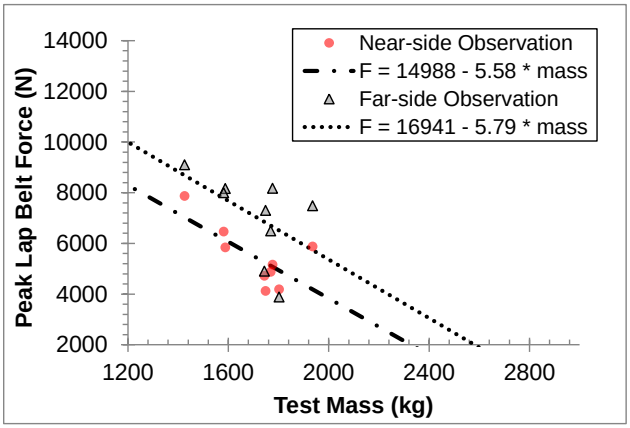

Figure 7. Relationship between lap belt load and vehicle mass.

Near-side Occupant Kinematics. In the LSI condition, the occupant in the driver's seat began moving directly forward with a gradually-increasing outboard translation. The frontal air bag was typically fully-deployed by the

time head contact was made, usually in the center or left-center of the bag. As the head contacted the frontal air bag, it continued to translate in an outboard direction, often having a rotational velocity about the local Z-axis induced as the face interacted with the frontal air bag. Contact with the side curtain varied greatly based on the vehicle and side curtain air bag design (Figure 25, APPENDIX H). In general, the head translated into the gap between the frontal air bag and the side curtain air bag and rotated about the local Y-axis. Depending on the extent of deployment and stiffness of the side curtain air bag, the head was either protected from contact (Accord, CX-5, and S60) or translated and rotated past the air bag and contacted the door panel (Fit, Mazda 3, and Forester).

In the RSI condition, the overall occupant kinematics were essentially a mirror-image of the kinematics in the LSI condition. As the occupant moved forward and to the right, the head interacted with the frontal air bag and translated to the right towards the gap between the frontal and side curtain air bags. However, in the case of the Accord, the side curtain air bag contacted the head before it interacted with the frontal air bag and imparted an outboard rotation about its the local Z-axis (Figure 8). The other RSI-P occupants showed similar kinematics to their LSI-D counterparts.

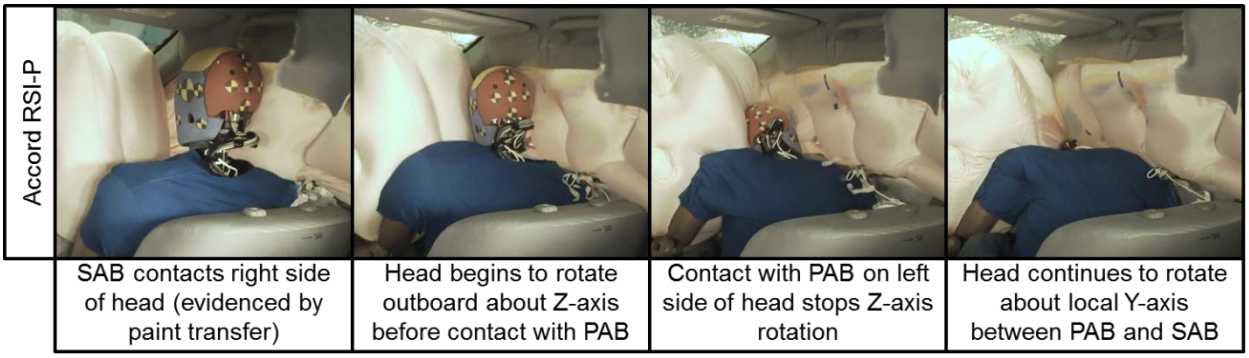

Figure 8. Kinematics of near-side occupant (RSI-P) in right-side impact test.

Far-side Occupant Kinematics. In the LSI condition, the far-side occupant was seated in the right front passenger seat. Like the near-side occupant location, the ATD began moving forward with an increasingly left lateral trajectory, inboard in this case. In all of the LSI vehicles, the frontal air bag appeared to be fully deployed by the time of head contact, and the head of the occupant contacted the left-hand side of the frontal passenger air bag. This contact initiated a positive Z-axis rotation of the head, and in all six of the LSI-P observations, the left side of the head contacted the center instrument panel (IP). In three of these six observations, contact was not evidenced by paint transfer but was apparent from high-speed video and head acceleration time-history (Figure 9). The peak head acceleration occurs in the Y-axis since it results from an impact to the side of the head, and occurs slightly after the peak head angular velocity since contact with the IP slows or stops the motion of the head. The earliest and most severe contact occurred in the Fit, where the head contacted the corner of a relatively narrow and visually stiff passenger air bag and rotated abruptly in the positive Z-axis direction to contact the center IP. On the other end of the spectrum was the CX-5, which had a wider and visually softer passenger air bag, which yielded under contact with the passenger's head until the point of maximum forward head excursion (Figure 10). Accordingly, out of all far-side occupants in this study, the Fit showed the highest head Z-axis angular velocity (4883 deg/s) while the CX-5 showed the lowest (1643 deg/s).

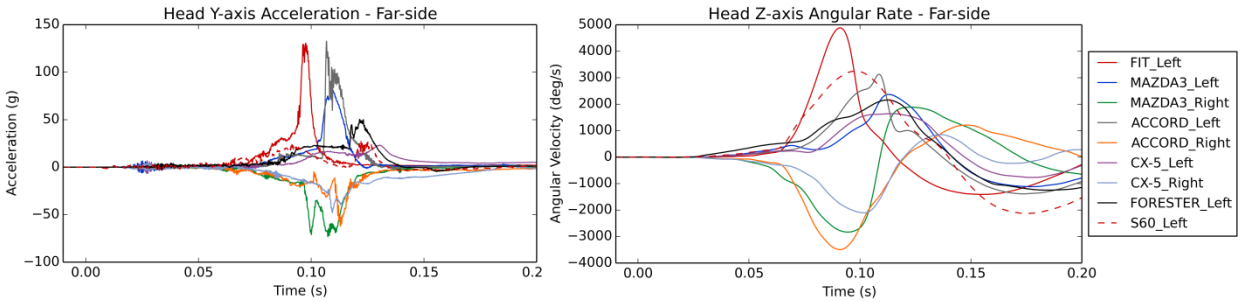

Figure 9. Y-axis head accelerations (left) and Z-axis angular velocities (right) of the far-side occupants.

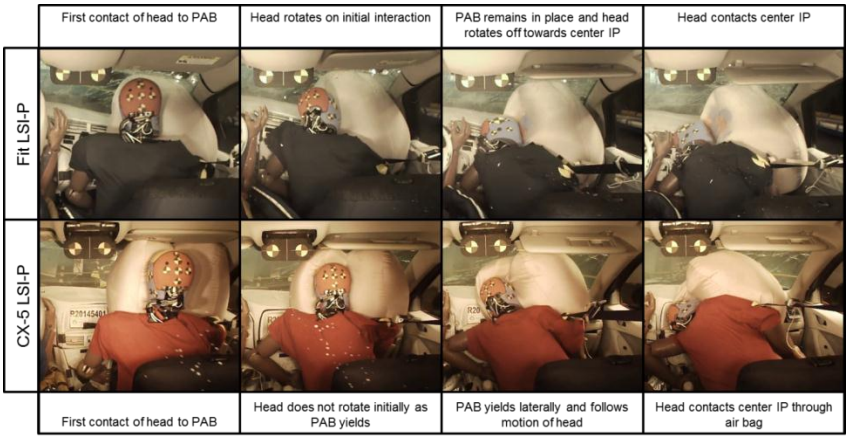

Figure 10. Kinematics of far-side occupant in left side impact test (LSI-P), comparing head rotation and center IP contact with different passenger air bag (PAB) designs.

In the RSI far-side condition, while the overall kinematics were a mirror-image of the LSI far-side condition, there were some localized changes due to differences in the driver-side and passenger-side restraints and interior features. The frontal air bag on the driver side was initially closer to the occupant but generally smaller and stiffer, so the initial interaction with the head may have differed from the passenger far-side condition. Also, since the hands of the driver were initially placed on the steering wheel, the right hand contacted the center IP and was subsequently impacted by the head in two of the three RSI-D observations. This did not occur for the passenger in the LSI far-side condition, as the hands of the passenger were initially placed on his lap. The differences in kinematics are shown in Figure 11 by presenting the LSI-P condition as-is and the RSI-D observation as a horizontal mirror-image at the same point in time during the crash. The head of the occupant in the RSI-D condition began rotating about the local Z-axis earlier and at a greater magnitude. This comparison is not too different from that shown in Figure 10, as the interaction of the RSI-D occupant with a stiffer, unyielding frontal air bag resulted in greater head rotational velocity and, visually at least, more forward and downward head excursion.

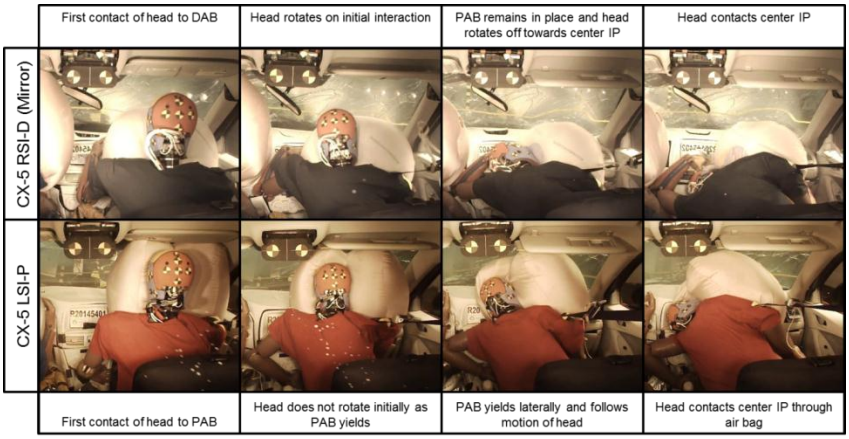

Figure 11. Comparison of the far-side driver and far-side passenger observations, taken at identical time steps during the test. Note that the RSI-D images are mirrored horizontally.

Occupant Injury Assessment.

For the purposes of this effort, occupant injury risk was assessed using the probability of an AIS $\geq$ 3 (or AIS $\geq$ 2 for the lower extremities) based on the injury criteria and underlying injury risk functions that can be applied to the THOR ATD. For the vehicles presented in Table 1 and Table 2, the body regions that showed the highest probability of injury include the brain (as predicted by BrIC), the chest (as predicted by the multipoint thoracic injury criterion), and the ankles (as predicted by ankle moment). These metrics show good agreement with the field injury exposure presented by Rudd et al. 2011 [6], where the body regions with the highest incidence of injury were the knee/thigh/hip, chest, lower extremity, and head. Summaries of the injury risk calculated by each criterion are

shown for the near-side (Table 5, APPENDIX D) and far-side (Table 6, APPENDIX E) occupants in the Appendix. This section will focus on the head, chest, knee/thigh/hip, and lower extremity. In the following bar charts, the shading of the bar represents the impact side (dark gray for left-side impact, light gray for right-side impact) while the fill pattern represents the occupant position (solid for near-side, cross-hatched far-side). RSI testing was not conducted for the Fit, Forester, and S60.

Head. Head injury predicted by the HIC_{15} and BrIC injury criteria are shown in Figure 12. The highest injury risk predicted by HIC_{15} occurs in the far-side condition, and three of the four observations above a 10 percent risk of AIS $\geq$ 3 injury occur in left-side impacts. Injury risk predicted by BrIC is notably higher, with a minimum of 23 percent risk AIS $\geq$ 3 injury in the Accord LSI-D observation. The average predicted BrIC injury risk for near-side occupants was 53 percent with five of the nine observations below a 50 percent risk of injury, while the far-side occupant average risk was 87 percent with all nine of the observations above a 50 percent risk of injury. The lowest-mass vehicles showed a higher injury risk as predicted by HIC_{15}, but there was no apparent relationship between BrIC and any vehicle structural response parameters. The measured BrIC value appears to be more sensitive to local interactions with the frontal air bags (as shown in **Figure 10**) and side curtain air bags than the differences in vehicle kinematics within the range of the current set of vehicles. Considering the three paired left-side to right-side comparisons, injury risk predicted by BrIC was higher in right-side impacts for all of the far-side occupants, while not consistently different for the near-side occupants.

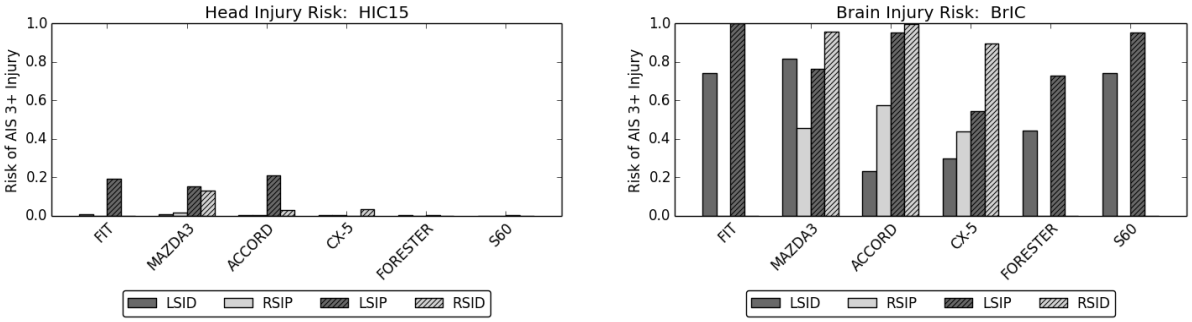

Figure 12. Risk of AIS ≥ 3 injury as predicted by HIC15 (left) and BrIC (right).

Chest. Chest injury risk presented in Figure 13 represent the injury risk predicted by the peak resultant chest deflection measured at any of the four rib deflection measurement locations on the THOR ATD at any point in time. This deflection is calculated as spatial resultant representing the length of the vector between the initial rib location and the current rib location, as measured in a coordinate system on the local spine segment. In all but one of the tests in this series (Fit LSI), chest deflection was higher for the near-side occupant than for the far-side occupant. Comparing left-side impacts to right-side impacts, all three near-side conditions showed a higher risk of chest injury in the right-side impact than the left-side impact, while the difference was not consistent for the far-side occupants.

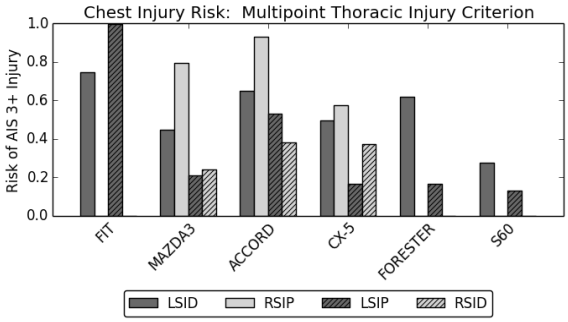

Figure 13. Risk of AIS ≥ 3 injury as predicted by multipoint thoracic injury criterion.

Knee/Thigh/Hip. While the axial load measured by the distal femur and the load measured at the acetabulum are intrinsically related due to the shared load path, the injury risk to the body regions in question is not necessary linearly related. This has been observed in field data, as only 50 percent of the occupants in oblique crashes who sustained pelvis and/or hip injury also sustained femur shaft fracture [6]. Femur fracture risk was generally low, with

only one observation predicting greater than a 10 percent risk of injury (S60 LSI-D) which resulted from compressive loading of the right femur. The risk of acetabulum fracture in the same observation was greater than 50 percent, also occurring in the occupant's right leg. Three out of the four highest acetabulum injury risks were predicted to the far-side occupant in a left-side impact (Figure 14).

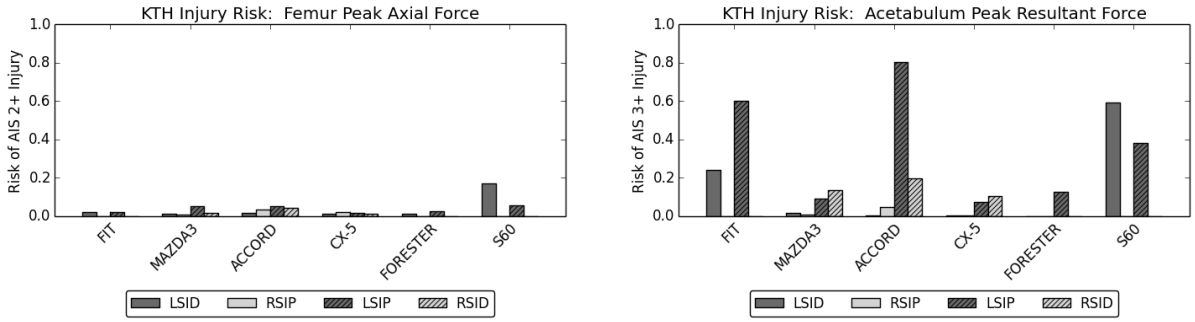

Figure 14. Risk of AIS ≥ 2/3 injury as predicted by femur axial force (left) and acetabulum force (right).

Lower Extremity. Risk of lower extremity injury was assessed using the Revised Tibia Index (RTI), which is summarized in Figure 15 as the maximum risk predicted using RTI for either the upper or lower tibia and either left or right leg. Injury risk predicted by RTI was generally low, with all but one observation predicting less than 25 percent risk of AIS ≥ 2 injury to the lower leg, specifically a tibia or fibula shaft fracture. The highest injury risk occurred again in the S60 LSI-D observation, again in the right leg which also saw a high risk of femur and acetabulum fracture. The S60 did have the highest right IP intrusion (see Figure 3), though this intrusion was only 22 millimeters. As shown in the past [5], the near-side occupant was expected to see a higher injury risk than the far-side due to intrusion into the occupant compartment. However, only five out of nine near-side occupants saw a higher injury risk than their far-side counterparts as predicted by RTI.

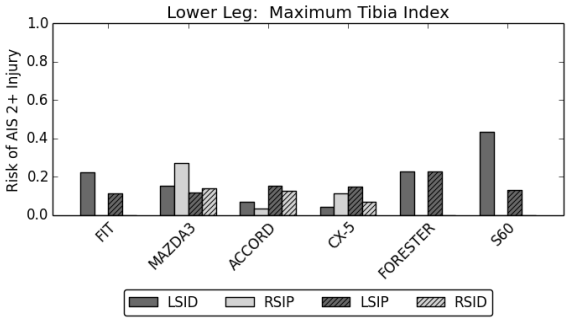

Figure 15. Risk of AIS ≥ 2 injury as predicted by Revised Tibia Index.

The prediction of ankle injury based on ankle moment was prevalent across all vehicles and occupant positions included in this study (Figure 16), especially due to ankle inversion/eversion. The average risk of ankle injury due to dorsiflexion moment was roughly 25 percent, while the average risk of ankle injury due to inversion/eversion moment was nearly 90 percent. Risk to near-side and far-side occupants were generally similar, as were risk of left and right ankle injury. Ankle inversion/eversion moment is generally induced by intrusion of the toe pan for the near-side occupant, as can be seen in high-speed video (Figure 26). However, high-speed video was not recorded in the far-side occupant seat position, so ankle kinematics can only be speculated based on occupant measurements. Another limitation in this assessment is that the tibia accelerations and lower tibia shear forces (FX, FY) were not measured in these tests due to channel count restrictions. However, based on the data presented by Kuppa et al. [16], the ankle moment measured at the lower tibia load cell may be an under-prediction of the peak ankle joint moment.

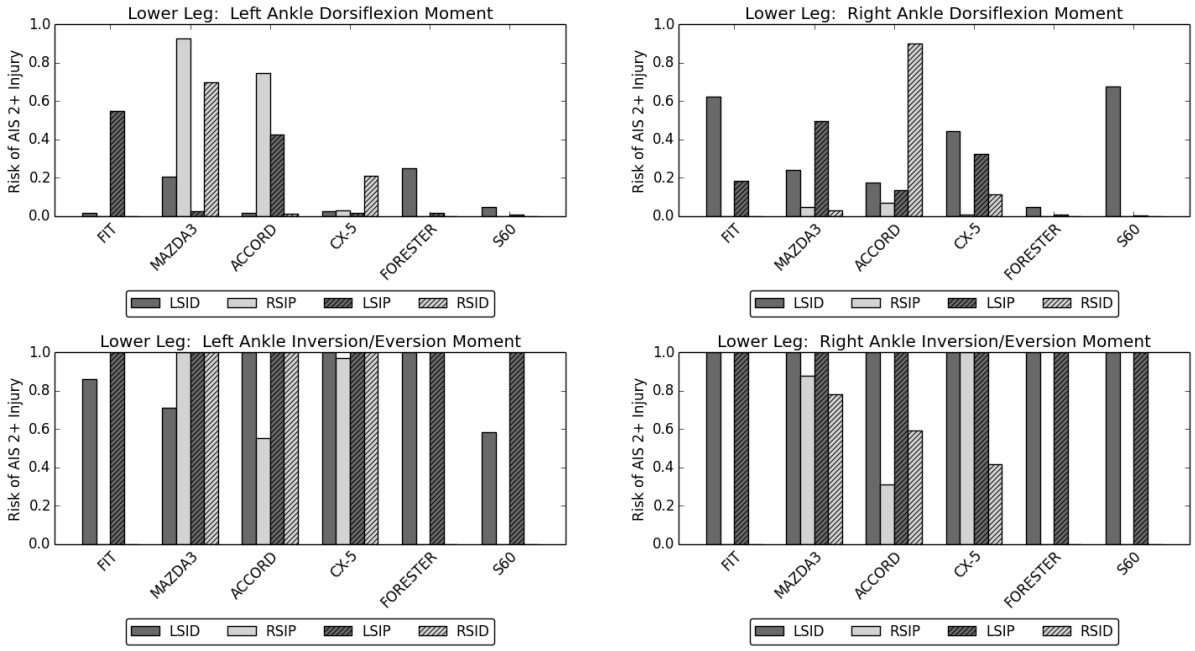

Figure 16. Risk of AIS ≥ 2 left and right ankle injury as predicted by ankle dorsiflexion (top) and inversion/eversion moment (bottom).

DISCUSSION

Vehicle Response

When comparing the intrusions of an LSI and RSI vehicle, the Accord had the greatest difference between left and right side (Figure 17). Figure 18 shows the post-test picture of the underbody for the Accord. The RSI picture was flipped in the figure to be able to make a better comparison. Figure 18 shows the Accord underbody had three different locations with different bending or pieces breaking off. The differences in this deformation may be due to the stack up of vehicle components on each side of the vehicle.

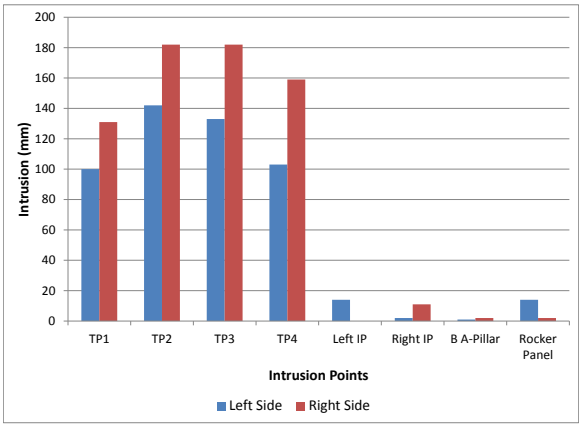

Figure 17 - Honda Accord interior intrusions

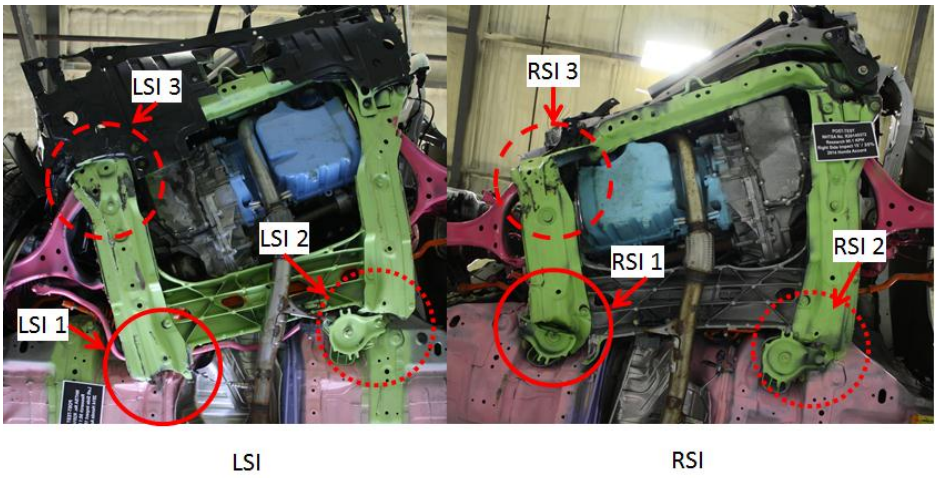

Figure 18 - Underbody of Honda Accord LSI and RSI

Occupant Response

Injury Risk. The current study implemented THOR ATDs to predict injury risk in a simulated frontal oblique impact for a group of nine vehicles. Overall, the highest probability of injury for both occupants in these nine vehicles was predicted to occur in the head, chest, and ankle. Correspondingly, the most frequently injured body regions in oblique crashes were the knee/thigh/hip, chest, leg/foot, and head, as presented by Rudd et al. [6]. While knee/thigh/hip injuries were not shown to have a proportionally high injury risk in the current set of tested vehicles, high acetabulum and femur forces consistent with a high risk of injury have been measured in previously-tested vehicles [5].

Ankle Injury. This test mode indicated a high risk of ankle injury, primarily due to ankle inversion and/or eversion as predicted by the ankle moment measured by the THOR ATD. These high ankle moments were induced by intrusion into the toe pan coupled with interaction with the pedals for the occupants in the driver's seat. However, there was no clear disadvantage to the driver seat location compared to the passenger seat location, nor to the inboard limb compared to the outboard limb. There was also no distinct correlation between peak intrusion and ankle injury risk, as highlighted by the fact that the Accord RSI-P seating location showed the largest toe pan intrusion (Figure 4), yet measured the lowest ankle inversion/eversion moment for both the left and right ankles (Figure 16).

Near-side versus Far-side. Visually, one of the key differences between the near-side and the far-side occupant kinematics is that the far-side occupant appears to slip out of the shoulder belt before the point of peak head excursion. One would expect to see a difference in the measured shoulder belt forces between the near-side and far-side occupants at the point that the shoulder appears to escape the shoulder belt, roughly 100 milliseconds after impact. However, the timing of shoulder belt unloading is similar between the near-side and far-side observations (Figure 6), which suggests that the shoulder escaping the shoulder belt does not mean that the shoulder belt is not still restraining the occupant. Instead, the shoulder belt loads the lower torso, evidenced by the lower left being the quadrant of peak chest deflection in 5 of the 6 LSI observations. Interestingly, the quadrant of peak chest deflection for the three RSI far-side observations is the upper right, perhaps a result of the arms being initially positioned with the hands on the steering wheel.

Another notable difference between the near-side and far-side occupant kinematics is the rotation of the head. This can be demonstrated by calculating the individual components of BrIC by dividing the peak angular velocity about each axis of the head by its respective critical value. In six of the nine near-side observations, the Y-axis angular rate is the peak axis of rotation (Figure 19, left), similar to what would be expected in a full-frontal impact. Peak angular rates for the far-side occupant are noticeably higher than those of the near-side occupant, and dominated by Z-axis angular rate for all far-side observations (Figure 19, right).

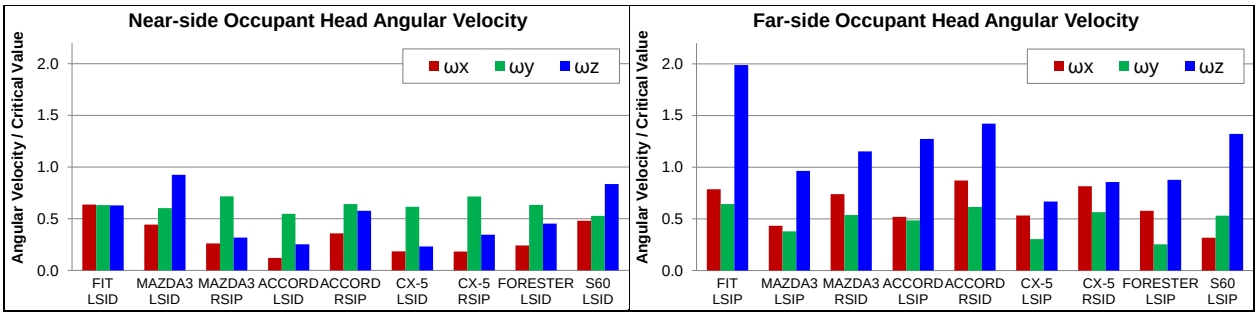

Figure 19. Components of head angular velocity for the near-side (left) and far-side (right) occupants.

LSI versus RSI. While the left-side and right-side impacts resulted in similar magnitudes of vehicle response, there were some differences in the occupant response that highlight important restraint system considerations. Comparing the three paired test conditions (Mazda 3, Accord, and CX-5 were all tested in both the LSI and RSI condition), the differences were more pronounced in the near-side occupant location than the far-side location. The far-side kinematics were generally a mirror image for the left- and right-side impacts, which can be seen in the head rotational velocity about the Z-axis (Figure 20, left). As the head interacted with the frontal air bag, it rotated outboard about its local Z-axis, resulting in positive angular velocity for the far-side passengers and negative angular velocity for the far-side drivers. However, the responses were not quite mirrored since the driver began to interact with the frontal air bag earlier than the passenger, with peak angular rates for the driver occurring earlier than their passenger counterparts in all three paired observations. The differences were less apparent for the near-side occupants (Figure 20, right), as the peak local Z-axis rotation was not consistently positive or negative for either group. Unlike the far-side occupant whose head interacted with only the frontal air bag, the head of the near-side occupant interacted with both the frontal air bag and the side curtain air bag. The driver-side frontal air bag and the passenger-side frontal air bag may have interacted with the side curtain air bag differently. Thus, it may be important to consider both left- and right-side oblique impacts in restraint system design.

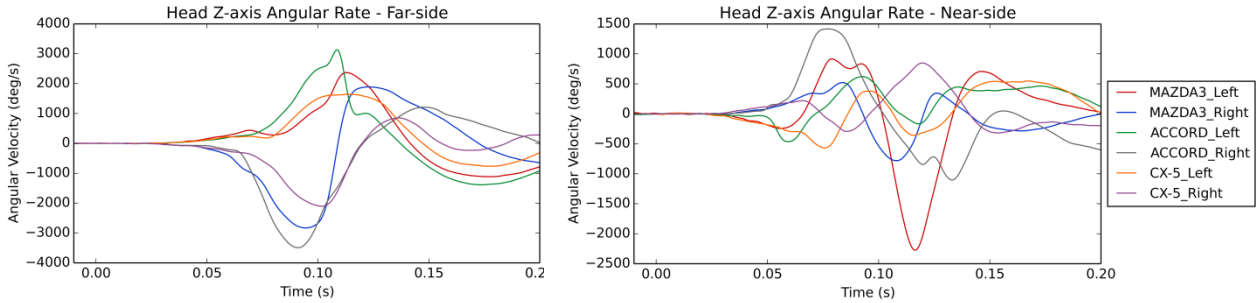

Figure 20. Comparison of head angular velocity in paired left- and right-side impact tests.

CONCLUSIONS

The interior intrusions on the toe pan increased moving toward the center of the vehicle and the highest point of intrusion on the toe pan was TP3. The deformation on the LSI and RSI can be different due to the stack up of non-symmetrical vehicle component layouts.

The current set of vehicles tested in the NHTSA Oblique condition suggest that additional countermeasures to reduce injury risk may be needed, despite these vehicles being rated "Good" or "Acceptable" in the IIHS Small Overlap Impact test condition and including side curtain air bags meeting the requirements set forth by FMVSS No. 226. The body regions for which the highest risks of injury were predicted were the head, chest, and lower extremity, consistent with injury incidence found in previously-published reviews of NASS and CIREN data. This study reviewed the differences between left-side and right-side impacts and found that neither was of notably higher risk, though there were localized differences in the interaction of the occupants with the frontal air bag. These differences were more pronounced in the near-side occupant location, where the interaction with the frontal air bag and side curtain air bag differed noticeably between left- and right-side impacts of the same vehicle design.

REFERENCES

1. Bean, J.D., et al., "Fatalities in Frontal Crashes Despite Seat Belts and Air Bags – Review of All CDS Cases – Model and Calendar Years 2000-2007 – 122 Fatalities," NHTSA Technical Report, Report No. DOT HS 811 202, September 2009.
2. Saunders, J., Craig, M. and Parent, D., "Moving Deformable Barrier Test Procedure for Evaluating Small Overlap/Oblique Crashes," SAE World Congress, paper no. 2012-01-0577, 2012.
3. Saunders, J., Craig, M. and Suway, J., "NHTSA's Test Procedure Evaluations for Small Overlap/Oblique Crashes," 22nd ESV Conference, Paper No. 11-0343, 2011.
4. Saunders, J. and Parent, D., "Repeatability of a Small Overlap and an Oblique Moving Deformable Barrier Test Procedure," SAE World Congress, paper no. 2013-01-0762, 2013.
5. Saunders, J. and Parent, D., "Assessment of an Oblique Moving Deformable Barrier Test Procedure," 23rd ESV Conference, Paper No. 13-0402, 2013.
6. Rudd, R., Scarboro, M., Saunders, J., "Injury Analysis of Real-World Small Overlap and Oblique Frontal Crashes," 22nd ESV Conference, Paper No. 11-0384, 2011
7. Ridella, S., Parent, D., "Modifications to Improve the Durability, Usability, and Biofidelity of the THOR-NT Dummy," 22nd ESV Conference, Paper No. 11-0312, 2011.
8. Lemmen, P., Been, B., Carroll, J., Hynd, D., Davidsson, J., Song, E., Lecuyer, E., "Development of an advanced frontal dummy thorax demonstrator," Proceedings of the 2012 IRCOBI Conference, 2012.
9. Törnvall, Fredrik. A New Shoulder for the THOR Dummy Intended for Oblique Collisions. Chalmers University of Technology, 2008.
10. AAAM: The Abbreviated Injury Scale – 1990, Update 1998. Des Plaines, Il. 2008.
11. AAAM: The Abbreviated Injury Scale – 2005, Update 2008. Des Plaines, Il. 2008.
12. Takhounts, E.G., Hasija, V., Moorhouse, K., McFadden, J., Craig, M., "Development of Brain Injury Criteria (BrIC)", Proceedings of the 57th Stapp Car Crash Conference, Orlando, FL, November 2013.
13. Crandall, J., "Injury Criteria Development: THOR Metric SD-3 Shoulder Advanced Frontal Crash Test Dummy," NHTSA Biomechanics Database, Report b11117-1, September 2013.
14. Parent, D., Craig, M., Ridella, S., McFadden, J., "Thoracic Biofidelity Assessment of the THOR Mod Kit ATD," 23rd Enhanced Safety of Vehicles Conference, Paper No. 13-0327, 2013.
15. Kuppa, S., Wang, J., Haffner, M., Eppinger, R., "Lower Extremity Injuries and Associated Injury Criteria," 17th ESV Conference, Paper No. 457, 2001.
16. Kuppa, S., Haffner, M., Eppinger, R., Saunders, J., "Lower Extremity Response And Trauma Assessment Using The THOR-Lx/HIIIr And The Denton Leg In Frontal Offset Vehicle Crashes," 17th ESV Conference, Paper No. 456, 2001.

APPENDIX A.

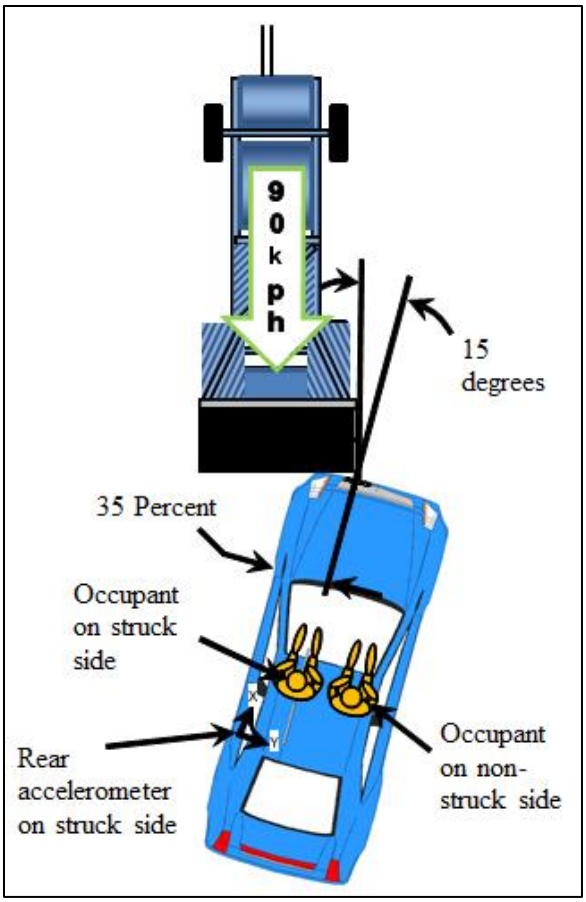

Figure 21. Test setup for Left Side Impact (LSI)

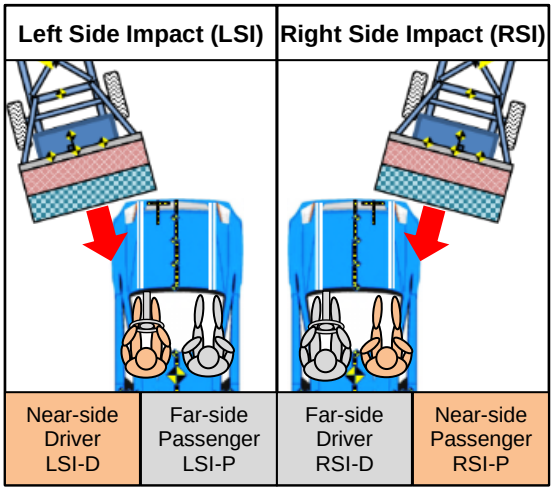

Figure 22. Occupant location terminology.

APPENDIX B.

Table 3. Intrusion Points

Description	Abbreviation	Figure
Left Footrest	TP1	Figure 23
Left Toe Pan	TP2	Figure 23
Center Toe Pan	TP3	Figure 23
Right Toe Pan	TP4	Figure 23
Left Instrument Panel	Left IP	
Right Instrument Panel	Right IP	
Center Steering Wheel	SW	
Bottom A-pillar	B A-pillar	Figure 24
Rocker Panel		Figure 24

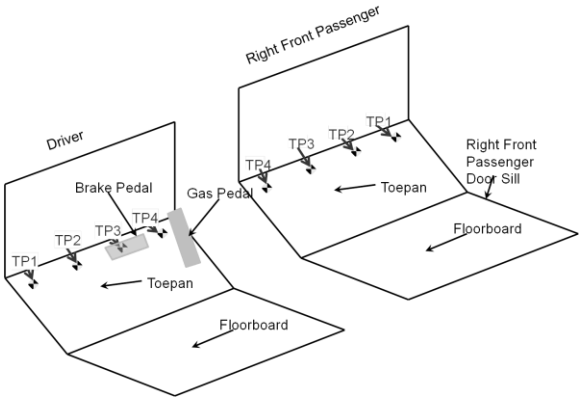

Figure 23: Interior intrusion measurements

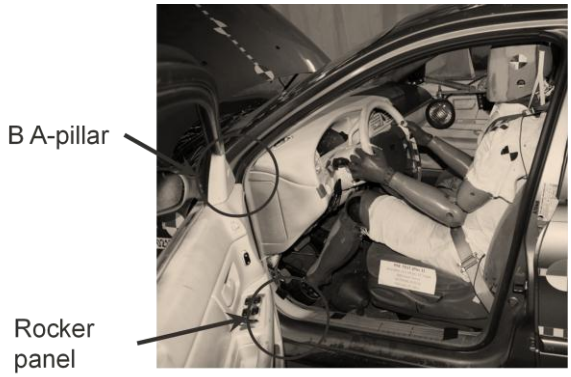

Figure 24: Location of B A-pillar and rocker panel intrusion points

APPENDIX C.

Table 4. Head contact locations and restraint deployment timing.

Mode	Vehicle	Contact Location (Evidence)	Frontal Air Bag Deployment	Side Curtain Air Bag Deployment	HIC15	Safety Belt Pretensioner
Left Front Driver						
LSI Oblique	Fit	AB (V, PT), SAB (V, PT), DP (V, PT)	AD (21)	AD (35)	264	AD (21)
	3	AB (V, PT), SAB (V, PT), DP (V, TAB)	AD (14)	AD (42)	268	AD (14)
	Accord	AB (V, PT), SAB (V, PT)	AD (16)	AD (46)	191	AD (18)
	CX-5	AB (V, PT), SAB (V, PT)	AD (13)	AD (43)	219	AD (13)
	Forester	AB (V, PT), SAB (V, PT), DP (V, PT)	AD (17)	AD (25)	193	AD (17)
	S60	AB (V, PT), SAB (V, PT)	AD (12)	AD (18)	152	AD (14)
RSI Oblique	3	AB (V, PT), IP (V, PT, TH)	AD (14)		750	AD (14)
	Accord	AB (V, PT), IP (V, PT)	AD (18)		419	AD (18)
	CX-5	AB (V, PT), IP (V, TH)	AD (12)		453	AD (12)
Right Front Passenger						
LSI Oblique	Fit	AB (V, PT), IP (V, PT)	AD (22)		910	AD (22)
	3	AB (V, PT), IP (V, TAB)	AD (16)		806	AD (13)
	Accord	AB (V, PT), IP (V, PT)	AD (18)		947	AD (18)
	CX-5	AB (V, PT), IP (V, TAB)	AD (15)		113	AD (15)
	Forester	AB (V, PT), IP (V, TAB)	AD (22)		200	AD (17)
	S60	AB (V, PT), IP (V, PT)	AD (14)		227	AD (15)
RSI Oblique	3	AB (V, PT), SAB (V, PT)	AD (14)	AD (42)	356	AD (14)
	Accord	AB (V, PT), SAB (V, PT), DP (V, PT)	AD (19)	AD (42)	190	AD (18)
	CX-5	AB (V, PT), SAB (V, PT)	AD (16)	AD (44)	247	AD (12)

AB	Air Bag	**AD ( )**	Available and Deployed (time deployed in ms)
SAB	Side Curtain Air Bag		
RR	Roof Rail	**AN**	Available and Not Deployed
IP	Instrument Panel	**N**	Not Available
DP	Door Panel		
V	Video		
PT	Paint Transfer		
TAB	Contact Through Air Bag		
TH	Contact Through Hand		

APPENDIX D.

Table 5. Summary of injury risk for near-side occupants in LSI and RSI Oblique crash tests

		Test Number	9043	8787	8999	8789	9042	8788	8998	8478	8488
		Vehicle Model	Fit	Mazda3	Mazda3	Accord	Accord	CX-5	CX-5	Forester	S60
		Impact Side	Left	Left	Right	Left	Right	Left	Right	Left	Left
		Occupant Location	D	D	P	D	P	D	P	D	D
Body Region	**Metric**	**AIS ≥ n**									
Head	HIC15	3	0.006	0.006	0.016	0.001	0.001	0.003	0.004	0.002	0.001
	BrIC	3	0.740	0.818	0.454	0.230	0.576	0.297	0.440	0.442	0.743
Neck	Nij	3	0.463	0.374	0.463	0.251	0.545	0.342	0.499	0.351	0.492
Chest	Multipoint Deflection	3	0.747	0.448	0.793	0.650	0.929	0.497	0.572	0.617	0.277
Abdomen	Peak Deflection	3	0.198	0.049	0.127	0.143	0.259	0.076	0.189	0.000	0.000
Left Leg	Acetabulum Force	2/3	0.241	0.000	0.005	0.000	0.049	0.000	0.001	0.000	0.003
	Femur Force	2	0.019	0.010	0.009	0.017	0.023	0.014	0.019	0.012	0.019
	Tibia Index, Proximal	2	0.026	0.008	0.223	0.029	0.030	0.030	0.113	0.046	0.006
	Tibia Index, Distal	2	0.028	0.021	0.273	0.035	0.032	0.035	0.035	0.115	0.017
	Tibia Proximal Force	2	0.005	0.004	0.001	0.005	0.003	0.004	0.001	0.002	0.006
	Tibia Distal Force	2	0.000	0.000	0.000	0.000	0.002	0.000	0.001	0.000	0.001
	Ankle Dorsiflexion Moment	2	0.858	0.711	1.000	0.999	0.555	1.000	0.970	1.000	0.584
	Ankle [in/e]version Moment	2	0.016	0.204	0.924	0.018	0.745	0.025	0.028	0.251	0.048
Right Leg	Acetabulum Force	2	0.001	0.016	0.006	0.001	0.033	0.003	0.003	0.000	0.590
	Femur Force	2	0.020	0.009	0.008	0.009	0.036	0.007	0.010	0.012	0.168
	Tibia Index, Proximal	2	0.144	0.075	0.069	0.015	0.010	0.032	0.016	0.041	0.143
	Tibia Index, Distal	2	0.221	0.153	0.020	0.069	0.006	0.044	0.022	0.226	0.433
	Tibia Proximal Force	2	0.010	0.002	0.001	0.004	0.003	0.003	0.002	0.003	0.003
	Tibia Distal Force	2	0.000	0.000	0.001	0.000	0.002	0.000	0.001	0.000	0.000
	Ankle Dorsiflexion Moment	2	1.000	1.000	0.876	1.000	0.309	1.000	1.000	1.000	1.000
	Ankle [in/e]version Moment	2	0.622	0.240	0.048	0.176	0.067	0.441	0.008	0.048	0.676

APPENDIX E.

Table 6. Summary of injury risk for far-side occupants in LSI and RSI Oblique crash tests

		Test Number	9043	8787	8999	8789	9042	8788	8998	8478	8488
		Vehicle Model	Fit	Mazda3	Mazda3	Accord	Accord	CX-5	CX-5	Forester	S60
		Impact Side	Left	Left	Right	Left	Right	Left	Right	Left	Left
		Occupant Location	P	P	D	P	D	P	D	P	P
Body Region	**Metric**	**AIS ≥ n**									
Head	HIC15	3	0.194	0.152	0.130	0.209	0.028	0.000	0.035	0.002	0.003
	BrIC	3	1.000	0.764	0.955	0.952	0.995	0.545	0.894	0.727	0.952
Neck	Nij	3	0.585	0.296	0.468	0.308	0.441	0.223	0.544	0.125	0.230
Chest	Multipoint Deflection	3	0.998	0.211	0.240	0.529	0.380	0.164	0.374	0.166	0.131
Abdomen	Peak Deflection	3	0.100	0.127	0.268	0.205	0.201	0.110	0.086	0.000	0.000
Left Leg	Acetabulum Force	2/3	0.271	0.014	0.136	0.804	0.000	0.001	0.106	0.125	0.382
	Femur Force	2	0.013	0.050	0.009	0.043	0.042	0.017	0.005	0.024	0.054
	Tibia Index, Proximal	2	0.114	0.117	0.140	0.010	0.128	0.146	0.035	0.228	0.092
	Tibia Index, Distal	2	0.103	0.036	0.105	0.153	0.050	0.114	0.000	0.084	0.128
	Tibia Proximal Force	2	0.001	0.001	0.002	0.003	0.006	0.001	0.004	0.003	0.002
	Tibia Distal Force	2	0.001	0.001	0.000	0.001	0.001	0.001	0.001	0.000	0.000
	Ankle Dorsiflexion Moment	2	1.000	1.000	1.000	1.000	1.000	1.000	0.000	1.000	1.000
	Ankle [in/e]version Moment	2	0.547	0.024	0.699	0.426	0.011	0.017	0.005	0.017	0.006
Right Leg	Acetabulum Force	2	0.600	0.090	0.005	0.024	0.198	0.072	0.006	0.009	0.364
	Femur Force	2	0.022	0.008	0.014	0.051	0.044	0.007	0.012	0.017	0.006
	Tibia Index, Proximal	2	0.028	0.062	0.038	0.002	0.045	0.090	0.014	0.048	0.098
	Tibia Index, Distal	2	0.027	0.045	0.014	0.010	0.023	0.114	0.000	0.138	0.115
	Tibia Proximal Force	2	0.002	0.001	0.003	0.004	0.003	0.001	0.004	0.002	0.004
	Tibia Distal Force	2	0.001	0.001	0.000	0.002	0.001	0.001	0.003	0.000	0.001
	Ankle Dorsiflexion Moment	2	1.000	1.000	0.782	1.000	0.593	1.000	0.414	1.000	1.000
	Ankle [in/e]version Moment	2	0.181	0.496	0.028	0.136	0.898	0.324	0.115	0.009	0.002

APPENDIX F.

Table 7. THOR-PMHS paired tests used in development of multipoint thoracic injury criterion.

Occupant Position	Environment	Restraint	Delta-V (km/h)	Age	Sex	Mass (kg)	Height (cm)	AIS 3+	PMHS BioDB	THOR BioDB	THOR Peak Res Defl (mm)
Front Driver	Gold Standard	3-point standard belt	10	59	F	80	167	No		11125	12.62
				69	M	84	178	No		11126	
				60	M	81	191	No			
Front Driver	Gold Standard	3-point standard belt	40	59	F	80	167	Yes		11123	49.4
				69	M	84	178	Yes		11124	
				60	M	81	191	Yes			
Front Passenger	1997 Ford Taurus	3-point force-limited belt plus air bag	48	57	M	70	174	No	8371	11129	51.3
				69	F	53	155	Yes	8372	11130	
				72	F	59	156	Yes	8373		
				57	M	57	177	No	8374		
Front Passenger	1997 Ford Taurus	Lap belt with air bag	48	40	M	47	150	Yes*	8377	11131	30.08
				70	M	70	176	No	8378	11132	
				46	M	74	175	No	8379		
Front Passenger	1997 Ford Taurus	3-point standard belt with air bag	48	55	M	85	176	Yes	8382	11127	54.83
				69	M	84	176	Yes	8383	11128	
				59	F	79	161	Yes	8384		
Front Passenger	1997 Ford Taurus	3-point standard belt	29	49	M	58	178	No		11133	42.75
				44	M	77	172	No		11134	
				39	M	79	184	No			
Front Passenger	1997 Ford Taurus	3-point standard belt	38	44	M	77	172	No		11135	51.17
										11136	
Front Passenger	Gold Standard 1	3-point standard belt	40	76	M	70	178	Yes	9546	11117	47.73
				47	M	68	177	Yes	9547	11118	
				54	M	79	177	Yes		11119	
				49	M	76	184	Yes			
				57	M	64	175	Yes			
				72	M	81	184	Yes	11014		
				40	M	88	179	Yes	11015		
				37	M	78	180	No	11016		
Front Passenger	Gold Standard 2	3-point force-limited belt	30	59	M	68	178	No		11120	26.78
				66	M	70	179	No		11121	
										11122	
Rear Passenger	2004 Ford Taurus	3-point standard belt	48	51	M	55	175	Yes	9337	11143	57.96
				57	F	109	165	Yes	9338	11144	
				57	M	59	179	Yes	9339	11145	
Rear Passenger	2004 Ford Taurus	3-point force-limited belt with pretensioner	48	67	M	71	175	Yes		11140	46.66
				69	M	60	171	No		11141	
				72	M	73	175	Yes		11142	
Rear Passenger	2004 Ford Taurus	3-point inflatable force-limited belt with pretensioner	48	72	M	88	173	Yes		11137	29.66
				69	M	69	175	No		11138	
				40	M	83	186	No		11139	

APPENDIX G.

Table 8. Summary of injury criteria and associated injury risk functions used to assess injury risk using THOR test results.

Criterion [ref]	Calculation	Vars	Variable Definition	Risk Function
HIC_{15}	$HIC_{15} = \left\lvert (t_2 - t_1)\left[\frac{1}{(t_2 - t_1)}\int_{t_1}^{t_2} a(t)dt\right]^{2.5}\right\rvert_{max}$	t_1	Beginning of time window in s	$p(AIS \geq 3) = \Phi\left[\frac{\ln(HIC_{15}) - 7.45231}{0.73998}\right]$
		t_2	End of time window in s	
		$a(t)$	Head CG resultant acceleration in Beginning of time window in g	
$BrIC$	$BrIC = \sqrt{\left(\frac{\max(\lvert\omega_x\rvert)}{\omega_{xC}}\right)^2 + \left(\frac{\max(\lvert\omega_y\rvert)}{\omega_{yC}}\right)^2 + \left(\frac{\max(\lvert\omega_z\rvert)}{\omega_{zC}}\right)^2}$	$\omega_{[x,y,z]}$	Angular velocity of the head about the local [x, y, or z] axis, in rad/s, filtered at CFC60	$p(AIS \geq 3) = 1 - e^{-\left(\frac{BrIC}{0.987}\right)^{2.84}}$
		$\omega_{[x,y,z]C}$	Critical angular velocities in rad/s	
		ω_{xC}	66.25 rad/s	
		ω_{yC}	56.45 rad/s	
		ω_{zC}	42.87 rad/s	
N_{ij}	$N_{ij} = \frac{F_z}{F_{zc}} + \frac{M_y}{M_{yc}}$	F_z	Z-axis force measured at upper neck load cell in N	$p(AIS \geq 3) = \frac{1}{1 + e^{3.227 - 1.969 N_{ij}}}$
		F_{zc}	Critical force (tension or compression) in N [2520/-3640]	
		M_y	Y-axis moment measured at upper neck load cell Nm	
		M_{yc}	Critical moment (flexion or extension) in Nm [48/-72]	
Multi-point Thoracic Injury Criterion	$R_{max} = max(UL_{max}, UR_{max}, LL_{max}, LR_{max})$ where $[U/L\lvert R/L]_{max} = max\left(\sqrt{[L/R]X^2_{[U/L]S} + [L/R]Y^2_{[U/L]S} + [L/R]Z^2_{[U/L]S}}\right)$	R_{max}	Overall peak resultant deflection in mm	$P(AIS \geq 3 \mid age, R_{max}) = 1 - exp\left(-\left[\frac{R_{max}}{exp(4.4853 - 0.0113age)}\right]^{5.03896}\right)$
		$[U/L\lvert R/L]_{max}$	Peak resultant deflection of the [upper/lower | left/right] quadrant in mm	
		$[L/R][X/Y/Z]^2_{[U/L]S}$	Time-history of the [left/right] chest deflection along the [X/Y/Z] axis relative to the [upper/lower] spine segment in mm	
Compression	$A_{max} = \frac{\max(\delta L, \delta R)}{d_{abd}}$	$\delta[L, R]$	Peak X-axis deflection of the left or right abdomen in mm	$p(AIS \geq 3) = 1 - e^{-\left(\frac{A_{max}}{0.4247}\right)^{3.6719}}$
		d_{abd}	Undeformed depth of the abdomen [238.4 mm]	
Acetabulum Load	$F_R = \sqrt{{F_x}^2 + {F_y}^2 + {F_z}^2}$	$F_{[x,y,z]}$	X-, Y-, and Z- axis force measured at the acetabulum load cell in kN	$p(AIS \geq 3) = \Phi\left[\frac{\ln(F_R/0.72) - 1.6526}{0.1991}\right]$
Femur Axial Load		F_z	Z-axis femur load in kN, filtered at CFC600	$p(AIS \geq 2) = \frac{1}{1 + e^{5.7949 - 0.5196 F_z}}$
Revised Tibia Index	$RTI = \frac{F}{F_c} + \frac{M}{M_c}$	F	Measured compressive axial force in kN	$p(AIS \geq 2) = 1 - exp\left(-exp\left[\frac{ln(RTI) - 0.2468}{0.2728}\right]\right)$
		F_c	Critical compressive axial force [12 kN]	
		M	Measured bending moment in Nm (resultant of medial-lateral and anterior-posterior directions)	
		M_c	Critical bending moment [240 Nm]	
Proximal Tibia Axial Force		F_z	Z-axis upper tibia load in kN, filtered at CFC600	$p(AIS \geq 2) = \frac{1}{1 + e^{5.6654 - 0.8189 F_z}}$
Distal Tibia Axial Force		F_z	Z-axis lower tibia load in kN, filtered at CFC600	$p(AIS \geq 2) = \frac{1}{1 + e^{4.572 - 0.670 F_z}}$
Dorsiflexion Moment	$M_{y_{ankle}} = M_Y - F_x D - \frac{m a_x D}{2}$	M_Y	Y-axis moment measured at lower tibia load cell in Nm	$p(AIS \geq 2) = \frac{1}{1 + e^{6.535 - 0.1085 M_y}}$
		F_x	X-axis force measured at lower tibia load cell in N	
		D	Distance between ankle joint and lower tibia load cell [0.0907m]	
		m	Mass between ankle joint and lower tibia load cell [0.72kg]	
		a_x	X-axis acceleration of the tibia in m/s^2	
Inversion/ Eversion Moment	$M_{x_{ankle}} = M_x - F_y D - \frac{m a_y D}{2}$	M_x	X-axis moment measured at lower tibia load cell in Nm	$p(AIS \geq 2) = \Phi\left[\frac{M_x - 40Nm}{10Nm}\right]$
		F_y	Y-axis force measured at lower tibia load cell in N	
		D	Distance between ankle joint and lower tibia load cell [0.0907m]	
		m	Mass between ankle joint and lower tibia load cell [0.72kg]	
		a_y	Y-axis acceleration of the tibia in m/s^2	

APPENDIX H.

Figure 25. Interaction of LSI-D occupants with driver air bag (DAB) and side curtain air bag (SAB).

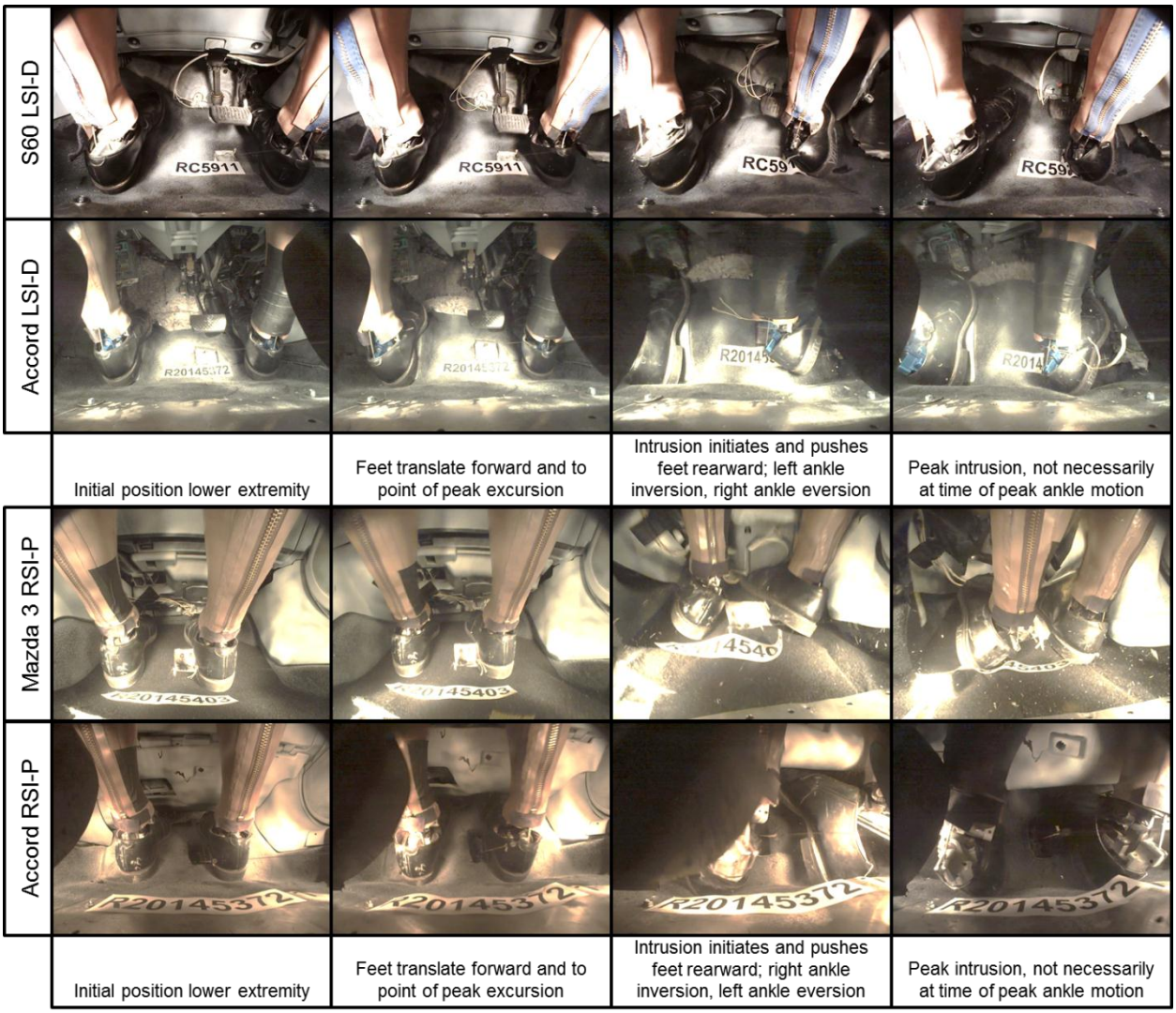

Figure 26. Lower extremity interaction with toe pan for vehicles with least (top of each pair) and most (bottom of each pair) toe pan intrusion.